The influence of scale on the air flow and pressure in the modelling of Oscillating Water Column Wave Energy Converters

Aggelos S. Dimakopoulos[1,*], Mark J. Cooker[2], Tom Bruce[3]

Abstract

In this work, air compressibilty effects are investigated during wave interaction with an Oscillating Water Column (OWC) Wave Energy Converter (WEC). Mathematical modelling includes a thermodynamic equation for the air phase and potential flow equations for the water phase. A simple three dimensional OWC geometry with a linear Power Take Off (PTO) response is considered and both the thermodynamic and potential flow equations are linearised. Analysis of the linearised system of equations reveals a nondimensional coefficient which we name "compression number". The flow potential is decomposed into scattering and radiation components, using an analogue of spring-dashpot response and taking into account the additional effects of air compressibility to wave interaction processes. We use these concepts to characterise the **relative importance of the air compressibilty effects** inside the OWC and to derive novel scaling relations for further investigation of scaling effects in OWC physical modelling. **The predictions of the methodology are validated against large scale experimental data, where compressibility effects are evident and further application of the methodology to a realistic OWC geometry**

*Corresponding author
Email address: A.Dimakopoulos@hrwallingford.com (Aggelos S. Dimakopoulos)
[1]Coastal Structures, HR Wallingford, Kestrel House, Howbery Park, Wallingford, OX10 8BA, UK
[2]School of Mathematics, University of East Anglia, Norwich Research Park, Norwich, NR4 7TJ, UK
[3]Institute for Energy Systems, School of Engineering, University of Edinburgh, King's Building, Edinburgh, EH9 3JL, UK

is used to demonstrate the importance of these effects to prototype scale.

Keywords: OWC, air compression, scaling effects, OWC performance, wave energy, WEC

1. Introduction

The oscillating water column (OWC) is arguably the most successful wave energy conversion (WEC) device, as its design and installation are relatively simple, and its maintenance is not demanding [1]. Wave interactions with these devices are critical for their performance and survivability. In the early study of Evans [2], the wave interaction of OWC devices is studied by considering a free-surface between (and the interaction with) two closely-spaced vertical plates[3]. In this model, the hydrodynamics inside the OWC are not completely resolved, as the water surface is treated as a horizontal rigid plate that oscillates vertically and the air pressure is modelled as a linear spring reacting to the rigid plate motion. The vertical motion of the mean water surface is the part of the internal wave motion that causes displacement of the air in the column above the surface. The other components of the free surface do not cause compression of the air above it. Given the assumptions above, the method can give predictions of the efficiency of the system, but not of hydrodynamic loads.

An attempt to quantify compression effects in OWC was made by Sarmento and Falcao [4], who analysed an ideal two-dimensional shallow-draught OWC and modelled the air phase as an ideal gas, with a linearised pressure - density relation. Due to the shallow-draught assumption, their analysis disregards the problem of interaction at the OWC entrance and it is considered that wave reflection originates from the back wall only. However, this is not the case for realistic OWC geometries, as usually the front wall at the entrance is immersed to ensure air entrapment under changing water levels due to e.g. tides, or storm surges. Nevertheless, the study does give useful insights for the causes of air compression in prototype OWC, demonstrating that these are more likely to

appear when the height of the OWC is increased. The nature of these effects is also studied, with respect to (i) the appearance of phase differences between free-surface flux and the pressure drop inside the chamber (causing additional wave energy to reflect back into the offshore environment), and (ii) the benefits of using turbines equipped with phase control to optimise energy absorption.

In [5], the potential flow equations are formulated for describing wave propagation from a far field and interaction with an OWC device, including the diffraction problem due to the immersed part of the front wall. The water is considered as an irrotational, inviscid fluid and, using the theoretical procedures developed in [6], [7] and [8], the method is capable of predicting the OWC efficiency and the development of linear sloshing modes inside the OWC chamber. However, the method of these authors treats the air as incompressible, so that the pressure drop from the air turbine is directly applied (as a boundary condition) at the free-surface. The analysis from [5] disregards the influence on the OWC efficiency of the compression of the air (inside the OWC) above the water and below the turbine. **Whilst the assumption may not be appropriate for all cases, particularly for full-scale OWC structures, the calculation method is an invaluable tool for determining the performance of OWC, in particular with respect to the optimisation of the OWC configuration (size of opening, layout cross-sectional area of the chamber, effect of wave collectors), given the incident wave characteristics. A recent example of such work is [9], where the introduction and influence of wave collectors in front of an OWC structure is studied, considering incompressible flow**.

In [10], the influence of the air compressibility in scaling an OWC physical model is discussed and the chamber height of the OWC is identified as a key parameter for scaling effects: keeping the chamber height constant ensures that compressible flow is appropriately scaled, thus confirming the analysis in [4]. As this requirement cannot always be met, alternatives are suggested, such as increasing the air volume or applying active pressure control. The influence of the air compressibility in the performance of the OWC is demonstrated, by the

numerical simulation of a reference OWC device, at full scale and at 1/10 scale. The numerical model is an extension of the method [5] to include compressibility effects at [11]. The results show that, at 1/10 scale, there are scaling effects due to air compressibility, which become more important as the pressure drop across the air turbine increases. Similar conclusions are also discussed in [12, 13], where dimensional analysis shows that, in order to eliminate air compressibility scaling effects, the air volume must be scaled with $(s_F)^2$, rather than $(s_F)^3$, where s_F is the Froude scale.

Compressible air flow in OWC chambers is studied further by Sheng et al. [14], assuming isentropic air flow. Their study does not consider the wave interaction problem, as the free-surface motion is represented as a rigid, flat boundary with a given first-order oscillatory motion. This allows them to decouple the equations of air motion from the wave motion and obtain a simple equation for volume flux through the turbine. They also take into account the different densities of the air inhaled from the atmosphere the air compressed inside the OWC and exhaled to the atmosphere. The air pressure drop is modelled as a quadratic dependence on the air volume flow rate. The main conclusions are (i) that the assumption of isentropic air compression is acceptable (because good agreement with experimental data is obtained), and (ii) that energy losses due to thermal processes are not significant. **More recently, the influece of the air humidity to the performance of OWC was discussed in [15]. The authors used a real gas methodology to calculate the thermodynamic properties for air - vapour mixtures and their theoretical model was validated against experiments. Initial results show that the influence of air humidity is significant, and further work is recommended towards this direction.**

Similar analysis is performed in [16] where they use linearised approach to derive a non-dimensional number (β) to characterise compressibility effects. This number can be used to assess the relative importance of compressibility effects with changing wave frequency, water density and OWC air column height. This non-dimensional number, however, does not include the influence of the

PTO resistance. The latter has an important effect on the evolution of air pressures and eventually the wave interaction processes with an OWC structure.

In [17] a numerical model is set-up using the Finite Element Method to study the interaction of a cylindrical floating OWC, as a single structure and a system of arrays. Their model was coupled with a linearised, isentropic state equation to include air compressibility. Their study showed that changing the air volume inside the OWC has a considerable influence on the performance of the OWC. In particular, carefully choosing the total air volume can be beneficial for the OWC performance, as it may increase the bandwidth of the power capture. By contrast, an inappropriate choice of air volume can significantly reduce the captured energy.

The objective of this paper is to study the compressibility effects and their impact on the performance of the OWC device within the context of the wave interaction problem. In a spirit similar to [18], we attempt to derive simple relations that will enable us to estimate these effects, in a way that can complement small-scale physical models, and numerical modelling using an incompressible solver. An additional goal is to provide some theoretical background for validating numerical models that include the compressibility of the air. A benefit is better designs of prototype OWC using small scale models, and recommendations about including air scaling in the design of small scale experiments. To achieve this, initially, the gas (air) flow problem will be investigated by applying a linear analysis to the 1D equations presented in [14]. The linear analysis is a well-know tool used to study OWC interaction with waves and air pressures [19], and despite the simplifiying assumptions excluding nonlinear and viscous effects, it has been proven a satisfactory tool to investigate these processes [20]. Subsequently, this analysis will be used in conjunction with potential flow theory, following a decomposition similar to that in [5]. **Using this decomposition as a starting point, we discuss the effect of air compressibility to energy efficiency, we investigate the effects of scaling on the air flow and pressure and we apply the analysis for characterising compressibility effects to realistic scenarios including experimental data [26, 24] and**

the OWC-WEC installed in Pico, Azores [30].

2. Air flow

2.1. Governing equations

Figure 1 shows a sketch of the domain in the vicinity of the OWC. For convenience, a 2D slice of a rectangular OWC is shown here, however, the analysis can be generalised to include additional OWC configurations, as shown further below. It is assumed that inside the OWC, the air water motion is governed by relations between quantities that primarily depend on time, that the air is well mixed so that it has a uniform temperature and pressure. The air-water motion is complicated by sloshing modes, but these cause zero net displacement; it is only the rise of the spatially averaged water level that can compress and displace the air-phase. There is no momentum transfer through viscosity at the air-water interface, as potential flow is assumed. The volume of air changes either due to discharge through the power take-off (PTO) or due to spring-like compression and expansion of the air.

The position of the PTO is not important for our study, but its resistance is, so we can conveniently define a resistance layer concept, where the PTO is replaced by an infinitely thin layer introducing the same pressure drop as the PTO. The extent of this layer covers a cross-sectional area of the OWC chamber, normal to direction of the air volume change. For OWC chambers where the cross-section does not change along the height (e.g. rectangular or cylindrical) this is the horizontal cross-sectional area of the chamber. For OWC chambers with smoothly varying horizontal cross-section, we may choose a characteristic cross-section, but to maintain consistency, we should define an effective height of the OWC by dividing the total volume of the air chamber in equilibrium conditions by the characteristic cross-sectional area.

A single parameter K for the resistance coefficient is used to calculate the pressure drop through the resistance layer. This resistance coefficient can be calibrated to represent the energy consumption of the PTO for any OWC con-

figuration. For the sake of clarity, energy consumption at the resistance layer corresponds to the total energy loss through the PTO, including viscous and turbulence losses at the turbine and power generation. Additional linear and turbulent losses (e.g inside the OWC chamber) could also be included in the calibration using available methodologies and / or experimental data. Scaling and assessment of linear losses have been further discussed in the literature e.g. [12], [20] .

At any instant we can divide the air in the OWC into infinitesimal columns of cross-sectional area $dA = dx \cdot dz$ (Figure 1). The volume, dV, of each column is:

$$dV = (h - \eta(x,t))dxdz \tag{1}$$

where $y = h$ is the top of the OWC; $y = \eta(x,t)$ is the free surface and t is the time. Subsequently, the total volume of air inside the OWC chamber is:

$$V(t) = \int \int_0^b dV = A_{OWC}h - \int \int_0^b \eta dxdz = A_{OWC}(h - \bar{\eta}(t)) \tag{2}$$

where the double-integrals are over the uniform cross-section of the OWC, A_{OWC} is the OWC cross-sectional area, $\bar{\eta}(t)$ is the spatially averaged water level inside the OWC. Throughout, an overbar denotes a spatially-averaged variable over cross-section of the resistance layer, which for our case study coincides with the actual OWC cross-section. Note that if the horizontal cross-section of the OWC chamber is not uniform along the y axis then A_{OWC} corresponds to a representative cross-sectional area and the height of the OWC must be defined as:

$$h = \frac{V_o}{A_{OWC}} \tag{3}$$

where is V_o is the static equilibrium value of $V(t)$. The equilibrium value of $\bar{\eta}(t)$ is zero.

Inside the OWC chamber, a uniform distribution of the relative air pressure $p(t)$ is assumed, in the following equation (4) of state for an ideal gas undergoing

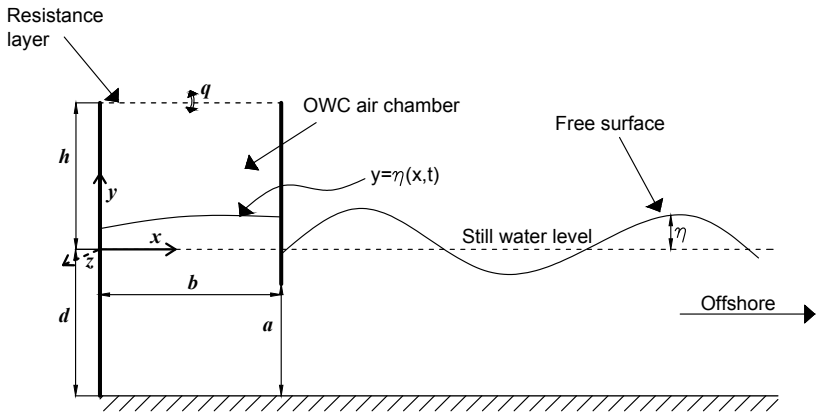

Figure 1: Geometry of OWC with an resistance layer. The position of the free surface and the air-water interface inside the OWC is $y = \eta(x, t)$. The side walls at $x = 0$ and $x = b$ are impermeable.

adiabatic, isentropic compression.

$$p = p_o \left(\left(\frac{\rho}{\rho_o} \right)^{\gamma} - 1 \right) \tag{4}$$

where $\rho(t)$ is the air density when the relative air pressure in the OWC chamber is $p(t)$, and the constant ρ_o is the equilibrium value for $\rho(t)$ under the equilibrium static atmospheric pressure p_o (note that the total pressure at any given time is $p(t) + p_0$). The polytropic expansion index γ for air has the value of $\gamma = 1.4$. Typical values for the air pressure and equilibrium density are p_o=1 atm and ρ_o=1.2 kg/m^3. The linearised version of equation (4) is given by:

$$p = \gamma p_o \left(\frac{\rho}{\rho_o} - 1 \right) \tag{5}$$

This approximation of (4) by (5) is satisfactory as long as there is a small enough deviation of ρ from ρ_o i.e. for $0.5 < \rho/\rho_o < 2$, the relative error will not exceed 15%. This approximation also ignores thermodynamic processes due to throttling effects in turbines and orifices [21], but in prototype structures, the extent of these effects is relatively local when compared to the total air volume inside the OWC chamber. Any additional energy losses caused by compressible throttling effects can be nevertheless included in the resistance layer coefficients, as long as relevant empirical relations are provided.

The uniformity of the density $\rho(t)$ lets us write the mass of air in the OWC as $m = m(t) = \rho(t)V(t)$. The flux of mass to and from the OWC, during inhalation, allows us to write:

$$\frac{dm}{dt} = \frac{d(\rho V)}{dt} = -\rho b \bar{v} \tag{6}$$

where $\bar{v}(t)$ is the spatially averaged velocity through the resistance layer ($\bar{v} < 0$ for inhale, $\bar{v} > 0$ for exhale), with respect to the cross-sectional are of the OWC for in 3D configurations or the width (per unit length in the z direction in Figure 1) in a 2D geometry. The velocity $\bar{v}$ is coupled with the pressure p, according to the PTO resistance characteristics for the resistance layer. Herein, we consider a quadratic relation between them:

$$p = K_1\bar{v} + K_2\bar{v}|\bar{v}| \tag{7}$$

where K_1 (kg·m^{-2}·s^{-2}) and K_2 (kg·m^{-3}) are coefficients of the resistance layer. **Equation 7 takes the form above because the pressure p must be an odd function of $\bar{v}$. After the first term containing a linear dependence (an odd function), the next order of term to choose is quadratic, but modified from v^2 to $\bar{v}|\bar{v}|$ to ensure the term is also odd. By having the pressure response as an odd function of the velocity, K_1 and K_2 can be considered positive, ensuring that energy is always absorbed at the PTO.**

Coefficients K_1 and K_2 are primarily representative of the PTO resistance, meaning the pressure drop induced by the flow rate passing through the PTO. The linear coefficient K_1 in particular is representative of the linear relation between the pressure drop and the discharge in Wells turbines [22]. The coefficient K_2 (with either K_1 zero or nonzero) is more representative of pressure damping configurations typically used in experiments to represent a PTO, e.g. the circular orifice in [23] or the rectangular one in [24] .

The solution of equation (7) with respect to $\bar{v}$ gives

$$\bar{v} = p\frac{1}{|p|}\frac{K_1}{2K_2}\left(\sqrt{1+\frac{4K_2}{{K_1}^2}|p|}-1\right) = \frac{p}{K(|p|)} \tag{8}$$

where

$$K(|p|) = |p|\frac{2K_2}{K_1}\frac{1}{\left(\sqrt{1+\frac{4K_2}{{K_1}^2}|p|}-1\right)} \tag{9}$$

and $\lim\{K\} = K_1$ as $K_2 \to 0$ and $\lim\{K\} = \sqrt{K_2|p|}$ as $K_1 \to 0$ and these limiting behaviours are consistent with equation (7) **when $K_2 = 0$ and K_1 nonzero, or when $K_1 = 0$ and K_2 nonzero respectively**. We next treat the flow with a linear analysis and in Section 2.4, consider the nonlinear (quadratic relation (7)) analysis for the resistance.

2.2. Linear analysis

We assume a linear response of the PTO resistance so that in (7) $K_2 = 0$ and introducing this as a limiting case in (9) results in $K(|p|) = K = K_1$. Hereafter we use the symbol K as K_1. We can also assume that $p << \gamma p_o$ and $\bar{\eta} << h$. Using these assumption and combiming equation (6) and (5) gives:

$$\frac{dp}{dt} + \frac{\gamma p_o}{hK} p = \frac{\gamma p_o}{h} \frac{d\bar{\eta}}{dt} \tag{10}$$

Equation (10) is valid both in 2D and 3D configurations, as K_1 and K_2 (and hence K) in equation (7) models the pressure drop with respect to the appropriate cross-sectional average velocity of the OWC. Equation 10 is essentially the same as the differential equation for pressure fluctuations in [25], derived in a similar line of reasoning and used for 2D and 3D cases.

We now assume that each variable (e.g. p, $\bar{\eta}$, $\bar{v}$) is time-periodic, has zero mean and shares a single frequency ω, and has a distinct phase constant. **The single frequency assumption is reasonable as, due to regular wave consideration, there is only one excitation frequency transmitted through the system. This is from the experimental data shown in Section 5 and similar rationale is also used by [14] and [16] in their analysis**. We can therefore write any such flow-variable f as:

$$f = f_c \mathcal{R}e\{e^{-i\omega t + i\alpha_f}\} \tag{11}$$

i is the imaginary unit, $f_c > 0$ the amplitude, and α_f the phase constant. The phase difference for the pressure α_p is set to zero and all other phase variables are calculated with respect to α_p. From this assumption, equation (10) gives the following relationship between the parameters:

$$p_c = \left(\frac{Ki\omega}{\frac{Ki\omega h}{\gamma p_o} - 1} \right) \bar{\eta}_c e^{i\alpha_\eta} \tag{12}$$

To eliminate the phase constant, we take the modulus of both sides to obtain:

$$\frac{p_c}{\bar{\eta}_c} = \frac{\gamma p_o}{h} \frac{\Omega}{\sqrt{\Omega^2 + 1}} = K\omega \frac{1}{\sqrt{\Omega^2 + 1}} \tag{13}$$

where

$$\Omega = \frac{K\omega h}{\gamma p_o} \tag{14}$$

We name this non-dimensional number, Ω, *the compression number* and discuss it in the next section. Also, considering the argument of both sides of equation (12) gives a relation between the phase constants:

$$\alpha_\eta = \frac{\pi}{2} - \alpha_\Omega \tag{15}$$

where:

$$\alpha_\Omega = \arctan(\Omega) \tag{16}$$

Let $Q = b\frac{d\bar{\eta}}{dt}$ and $q = b\bar{v}$ denote the volumetric flux of the displaced air due to the interfacial motion and air flow at the resistance layer, respectively. Using equations (8) and (11), the amplitudes $Q_c = b\eta_c\omega$ and $q_c = bp_c/K$ are calculated and equation (13) implies

$$\Pi = \frac{q_c}{Q_c} = \frac{1}{\sqrt{\Omega^2 + 1}} \tag{17}$$

where Π expresses the ratio of the volume flux through the resistance layer to that displaced by the water surface. Owing to equation (8), $\alpha_q = 0$ and from the relation between $\bar{\eta}$ and $d\bar{\eta}/dt$ we have: $\alpha_Q = \alpha_\eta - \frac{\pi}{2}$. Comparing with (15) we deduce:

$$\alpha_Q = -\alpha_\Omega \tag{18}$$

Hence the phase difference between the volume flux at water surface is according to equation (18).

2.3. Characterisation of air flow

The compression number Ω can be considered as a parameter that measures the relative importance of air compressibility, with respect to the OWC characteristics. The definition (14) shows that Ω depends on the OWC height, the

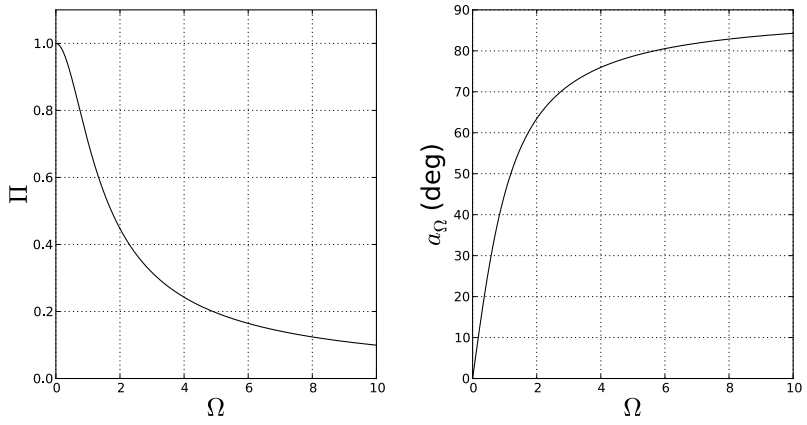

Figure 2: Variation with respect to Ω of volume flux ratio Π and phase difference α_q

wave frequency, and the PTO resistance. Quantities such as Π in equation (17) and α_q in equation (18) depend on Ω, as shown in Figure 2.

Taking into account the analysis in the previous sections and observations from Figure 2, the behaviour of the OWC system can be characterised using the compression number Ω. In particular:

- For $\Omega \simeq 0$ (incompressible behaviour) the air volume fluxes at the water level and at the resistance layer have the same amplitude and they are in phase. This suggests that the air is behaving as an incompressible fluid.

- For $\Omega >> 0$ (compressible behaviour), there is less volume flux passing through the resistance layer than that displaced by the water surface. In addition, the phase difference increases from 0 between the two volume fluxes as the value of Ω increases. As Ω increases from zero, compression becomes more important.

- As $\Omega \to \infty$ the behaviour becomes that of a closed OWC chamber. If Ω=2 this is already a large value and little air is passing through the PTO. However, there can still be volume displacement at the free-surface,

depending on the compressibility of the gas. The phase difference α_Ω is $\pi/2$, and the system behaves as if the chamber is fully closed.

The distinction between compressible and incompressible regimes should be made on the grounds that Ω is sufficiently small for air compressibility to matter. It is therefore proposed that this treshold is set to $\Omega \leq 0.1$, as in this case $\Pi > 0.95$ and $\alpha_\Omega < 10^o$.

The observations above indicate that for a given gas, the flow characterisation depends on the combination of the OWC dimensions, the PTO resistance and the incident wave conditions. Taking the two extreme cases $\Omega = 0$ and $\Omega = \infty$ and considering the pressure inside the OWC, it can be shown through the previous analysis that:

$$p = \begin{cases} K\frac{\partial \bar{\eta}}{\partial t} & \text{for} \quad \Omega = 0 \\ \frac{\gamma p_o}{h}\bar{\eta} & \text{for} \quad \Omega \to \infty \end{cases} \tag{19}$$

Therefore, it can be hypothesised that when the air behaves as incompressible, ($\Omega = 0$) the response of the OWC to the free-surface motion can be described as a dashpot that consumes energy from the free-surface oscillation, and when $\Omega = \infty$, the response of OWC can be described as a spring that temporarily converts kinetic energy to potential energy of compression, while not extracting any total energy from the system. It is therefore reasonable to suggest that for $0 < \Omega < \infty$, the response of OWC is that of dashpot-spring system that is shown in Figure 3.

Considering $\bar{\eta} = \eta^I + \eta^C$, where η^I and η^C are the free surface elevation related to the incompressible mode (dashpot response) and the compressible mode (spring response) of the overall free-surface oscillation. Noting that in such a system, the spring and dashpot motions will have a $\pi/2$ phase difference, we can establish a trigonometric relation between the total amplitude η_c and the amplitudes of each mode, η_c^C and η_c^I, such as:

$$\frac{\eta_c^C}{\eta_c^I} = \Omega = \tan(\alpha_\Omega) \tag{20}$$

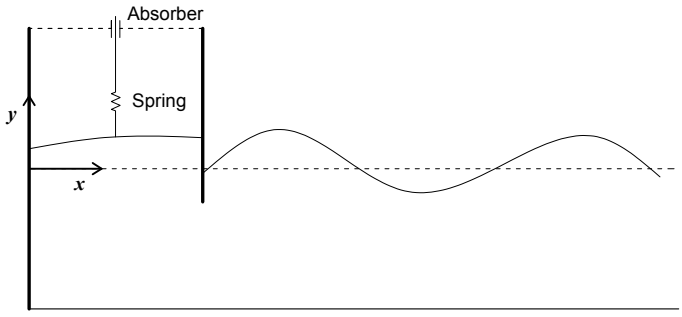

Figure 3: Spring dashpot analogy for OWC response to free-surface oscillation

and

$$\eta_c = \frac{\eta_c^C}{\sin\alpha_\Omega} = \frac{\eta_c^I}{\cos\alpha_\Omega} \tag{21}$$

Note also that

$$\sin\alpha_\Omega = \frac{\Omega}{\sqrt{1+\Omega^2}} \qquad \text{and} \qquad \cos\alpha_\Omega = \frac{1}{\sqrt{1+\Omega^2}} \tag{22}$$

Distinguishing between the incompressible and the compressible mode is a key element for performing the wave interaction analysis and investigating scaling effects. For example, the incompressible mode is responsible for power generation, and isolating its interaction from the incident wave field is useful to understand the effect of scaling on energy production.

The concept of the compression number and its importance for characterising air flow inside the OWC chamber can be also assessed by comparing it to the non-dimensional number derived by [16], defined according to the following:

$$\beta = \frac{\omega^2 V_o \rho_w}{{c_o}^2 b \rho_o} \tag{23}$$

where ρ_w is the air density and c_o the speed of sound. Given that ${c_o}^2\rho_o = \gamma p_o$ and $V_o/b = h$ then β compares to Ω as follows:

$$\beta = \Omega\frac{\omega\rho_w}{K} \tag{24}$$

By definition, parameter β includes the influence of the water density and neglects the effect of the PTO resistance, as opposed to Ω. Differences in sea and fresh water densities are typically taken into account as a scaling effect when modelling wave structure interaction problems, but these generally less than 3%. By contrast, the influence of the PTO resistance to air scaling effects is more significant, especially for studies verifying the design of the OWC, as typically in these studies, a number of different of PTO resistance coefficients might be considered and the importance of scaling effects will be different for each K. We therefore believe that Ω is more helpful than β for indicating the importance of

air compressibility during the design stage of an OWC. The influence on scaling due to change in water density will be further discussed in Section 4, where scaling relations are derived.

2.4. Quadratic resistance

OWC devices are usually mounted with Wells turbines that have a linear velocity-pressure relation for the PTO resistance [22], although it is common practice to employ quadratic relations to describe the resistance relation for physical modelling purposes [26, 14]. However, using equation (7) with $K_2 \neq 0$ would make impossible the use of a simple non-dimensional number to characterise the air flow inside the OWC. In order not to lose this advantage, we can write equation (7) as follows:

$$p = (K_1 + K_2|\bar{v}|)\,\bar{v}. \tag{25}$$

Now, we attempt a linearisation of (25) which includes the influence of the variable term in the brackets. A representative approximation comes from considering the period-averaged value for $|\bar{v}|$, which we write as:

$$\bar{v}_m = \frac{1}{T}\int_0^T \bar{v}_c|\cos\omega t|dt = \frac{2}{\pi}\bar{v}_c \tag{26}$$

where $\bar{v}_m$ is the time-average value over the period $T = 2\pi/\omega$. Replacing the time-varying $|\bar{v}|$ with the constant $|\bar{v}_m|$ in equation (25) gives the linear approximation:

$$p = K_3\bar{v} \tag{27}$$

where $K_3 = K_1 + K_2\bar{v}_m$. Our linearisation of equation (25) is graphically represented in Figure 4. The straight line is closer to the dashed curve over a wider range of $\bar{v}/\bar{v_c}$ than using a straight line through the origin that it tangent to the curve. Our linearisation (27) is better than simply approximating (25) by $p = K_1\bar{v}$. **Using the K_2 linearisation can be nevertheless not practical on occasions where velocity data are not provided for the**

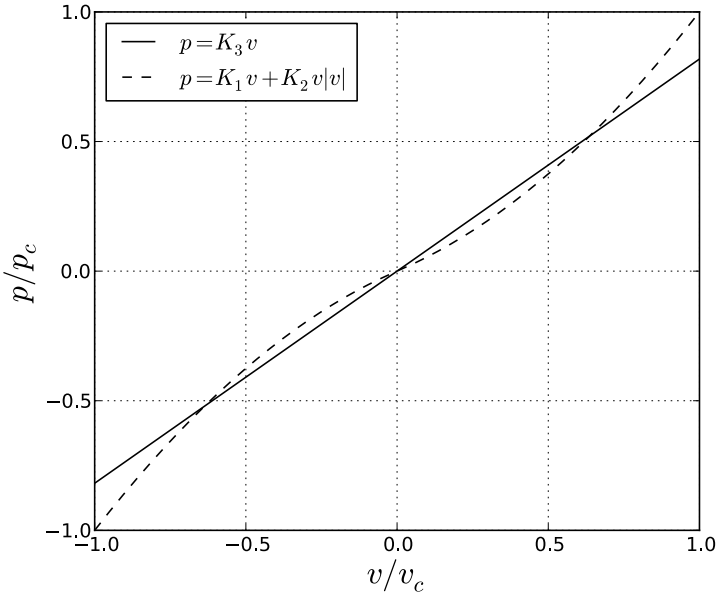

Figure 4: Linearisation of the resistance relation

OWC structure in question. In this case, an estimate of the velocity at the orifice can be provided from approximate relations, as shown in Section 5.

3. Wave interaction

3.1. Potential flow equations

The geometry of the domain around the OWC device is shown in Figure 5, where the subdomains for the air and water and their boundaries are identified. In the air subdomain, inside the OWC, the flow is governed by equation (10), while in the water subdomain, linearised potential flow theory is used. We assume that plane regular waves approach under normal incidence and interact with the rectangular OWC chamber. The flow in the water subdomain is two-dimensional ($x - y$ plane). This does interfere with the assumptions on the

configuration of the OWC chamber which can be either 2D or 3D. Herein, for simplicity, we assume that the OWC is rectangular, although the methodology can cover any OWC configuration, as long as the conditions stated in Section 2 are respected.

Considering the potential flow theory for the water subdomain ($-d \leq y \leq 0$), the flow is governed by Laplace's equation:

$$\frac{\partial^2 \Phi}{\partial x^2} + \frac{\partial^2 \Phi}{\partial y^2} = 0 \tag{28}$$

where $\Phi = \Phi(x, y, t)$ is the velocity potential. Neglecting surface tension and shear stress effects, the linearised dynamic boundary condition at $y = 0$ is:

$$\frac{\partial \Phi}{\partial t} + g\eta = \begin{cases} 0 & \text{for} \quad x \geq b \quad \text{(outside the OWC)} \\ -\frac{p}{\rho_w} & \text{for} \quad 0 \leq x \leq b \quad \text{(inside the OWC)} \end{cases} \tag{29}$$

where ρ_w is the water density and g the gravitational acceleration. Assuming linear flow dynamics, the linearised kinematic boundary condition at the free-surface and at the air-water interface is:

$$\frac{\partial \Phi}{\partial y} = \frac{\partial \eta}{\partial t} \quad \text{at } y{=}0 \text{ for } x \geq 0 \tag{30}$$

Combining the dynamic and the kinematic boundary conditions gives:

$$\frac{\partial^2 \Phi}{\partial t^2} + g\frac{\partial \Phi}{\partial y} = \begin{cases} 0 & \text{for} \quad x \geq b \quad \text{(outside the OWC)} \\ -\frac{1}{\rho_w}\frac{\partial p}{\partial t} & \text{for} \quad x \leq b \quad \text{(inside the OWC)} \end{cases} \tag{31}$$

We can manipulate equations (29)-(31) to remove the time dependency by assuming time-periodic motion at one frequency ω. Using the linear analysis of section 2.2, we can include the phase differences between p and η, but now with the loss of generality, we set $\alpha_\eta = 0$ and $\alpha_p = \alpha_\Omega - \pi/2$. Thus:

$$\begin{aligned} &\eta(x,t) = \eta_c(x)e^{-i\omega t} \\ &\Phi(x,y,t) = \phi(x,y)e^{-i\omega t} \\ &p(t) = p_c e^{-i\omega t - i(\pi/2 - a_\Omega)} = p_c \sin(\alpha_\Omega)e^{-i\omega t} - ip_c \cos(\alpha_\Omega)e^{-i\omega t} \end{aligned} \tag{32}$$

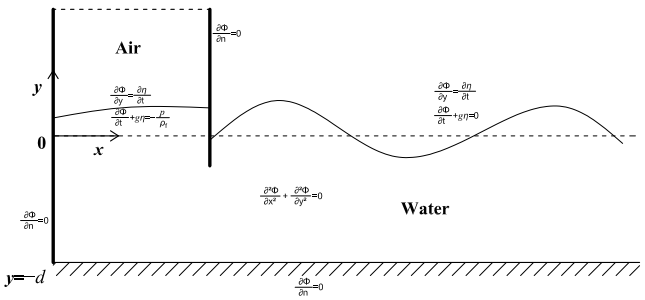

Figure 5: Potential flow equations in the fluid subdomain for the velocity potential Φ of the water flow.

By substituting equations (32) into (31) and taking into consideration equation (22)

$$-\frac{\omega^2}{g}\phi+\frac{\partial\phi}{\partial y}=\begin{cases}0 & \text{for} \quad x\geq b\\ \frac{\omega}{\rho_w g}\frac{p_c}{\sqrt{1+\Omega^2}}+i\frac{\omega}{\rho_w g}\frac{\Omega p_c}{\sqrt{1+\Omega^2}} & \text{for} \quad 0\leq x\leq b\end{cases} \tag{33}$$

Equation (33) can be decomposed to scattering and radiation components, as shown in [5]. Following a similar procedure, the flow potential, ϕ is decomposed into: i) the scattering potential, ϕ^S, which describes the fully reflective case of wave interaction with the OWC fully open ($p = 0$) and (ii) the radiation potential ϕ^R, which describes the wave radiation for the pressure applied in the OWC. Including the air compression effects, the radiation potential can be further decomposed into ϕ^{RI} (incompressible radiation) and ϕ^{RC} (compressible radiation).

$$\phi=\phi^S-\phi^{RI}-\phi^{RC} \tag{34}$$

Similar to [5], the dynamic boundary condition (33) is decomposed as follows:

$$\begin{aligned}
&-\tfrac{\omega^2}{g}\phi^S+\tfrac{\partial\phi^S}{\partial y}=0\\
&-\tfrac{\omega^2}{g}\phi^{RI}+\tfrac{\partial\phi^{RI}}{\partial y}=\begin{cases}0 & \text{for} \quad x\geq b \quad \text{(outside the OWC)}\\ \frac{\omega}{\rho_w g}p^I & \text{for} \quad 0\leq x\leq b \quad \text{(inside the OWC)}\end{cases}\\
&-\tfrac{\omega^2}{g}\phi^{RC}+\tfrac{\partial\phi^{RC}}{\partial y}=\begin{cases}0 & \text{for} \quad x\geq b \quad \text{(outside the OWC)}\\ \frac{\omega}{\rho_w g}p^C & \text{for} \quad 0\leq x\leq b \quad \text{(inside the OWC)}\end{cases}
\end{aligned} \tag{35}$$

where

$$\begin{aligned}
p^I&=\tfrac{p_c}{\sqrt{1+\Omega^2}}\\
p^C&=i\tfrac{\Omega p_c}{\sqrt{1+\Omega^2}}
\end{aligned} \tag{36}$$

In equation (35), the scattering potential is dependent on the incident wave conditions, the width of the OWC, b, and the entrance immersion depth, a, and corresponds to the excitation of the internal free surface of the OWC from an incident wave field. The incompressible radiation potential corresponds to a motion of the OWC free-surface which radiates as a wave field outside of

the OWC. On removing the radiation from the scattering potential, the wave field and associated OWC free-surface motion for the fully coupled problem is derived. The compressible radiation potential then corresponds to the problem of a free oscillation of the free surface of an OWC with capped PTO. Among the three potentials, only in the incompressible radiation case the net flux of energy change is non-zero. So, strictly speaking, the ϕ^{RC} does not involve any energy radiation, however, we keep this naming convention for convenience. In equation (35) the velocity potential is a complex quantity ($\phi(x,y) = cR(x,y)$, where c is a complex number constant describing phase α_ϕ and $R(x,y)$ is a real function), despite removing the time dependency, as there are still phase differences between the three components.

Assuming that the y-dependence is the same for ϕ^{RI} and ϕ^{RC}, both inside and outside the OWC, in (35), it can be demonstrated that:

$$\phi^{RC} = i\Omega\phi^{RI}. \tag{37}$$

Volume fluxes at the free-surface in the OWC can be derived by integrating the vertical velocity of the air-water interface with respect to $x \in [0, b]$. Using the decomposition of the potentials, the three time-independent amplitudes of free-surface fluxes $q_c^S, q_c^{RI}, q_c^{RC}$, corresponding to the scattering, incompressible radiation and compressible radiation potential, respectively, are defined as:

$$q^{S,RI,RC} = \int_o^b \frac{\partial\phi}{\partial y}^{S,RI,RC} dx \tag{38}$$

Using the same approach, we can also calculate the fluxes q^I and q^C corresponding to the incompressible and compressible modes derived from the spring and dashpot analogue (see Section 2.3) as follows:

$$q^{I,C} = \int_o^b \frac{\partial\phi}{\partial y}^{I,C} dx \tag{39}$$

where ϕ^I and ϕ^C are the velocity potentials satisfying the incompressible and compressible modes, respectively. Following the argument in [5], to obtain the total flux we must remove the radiation flux from the scattering flux. In our case, we argue that by removing the incompressible or compressible radiation fluxes

(q^{RI} and q^{RC}) from a certain proportion of the scattering flux q^S, we obtain the fluxes related to the incompressible (dashpot) or compressible (spring) modes, q^I and q^R, respectively.

$$q^I = \Lambda^I q^S - q^{RI} \tag{40}$$

$$q^C = \Lambda^C q^S - q^{RC} \tag{41}$$

where complex constants Λ^I and Λ^C are scaling coefficients of the scattering flux. These coefficients represent the ratio of the incident wave field that excites the incompressible and the compressible modes respectively. Since the proportions of the scattering fluxes add up to the total flux, it is therefore evident that:

$$\Lambda^I + \Lambda^C = 1 \tag{42}$$

We can calculate Λ^I and Λ^C by finding relations between the fluxes in equations (40) (41). Using the definition $\eta = \eta^I + \eta^C$ within the context of complex exponential functions and taking into account the analysis in section 2.3, we define:

$$\eta^C = i\Omega\eta^I \tag{43}$$

Equation (43) shows that the phase of η^C precedes the phase of η^I by $\pi/2$. Translating equation (43) to a relation between fluxes gives:

$$q^C = i\Omega q^I. \tag{44}$$

Combining equations (37) and (38), we find

$$q^{RC} = i\Omega q^{RI}. \tag{45}$$

Combining equations (40, 41, 42, 44 and 45) we obtain the pair of relations

$$\begin{aligned} \Lambda^I &= \tfrac{1}{1+\Omega^2} - i\tfrac{\Omega}{1+\Omega^2} \\ \Lambda^C &= \tfrac{\Omega^2}{1+\Omega^2} + i\tfrac{\Omega}{1+\Omega^2}. \end{aligned} \tag{46}$$

Coefficients Λ^I and Λ^C are complex numbers, as they incorporate the phase differences between fluxes. Also (46) implies that $|\Lambda^I|^2+|\Lambda^C|^2 = 1$, which shows that the coefficients satisfy the energy balance for the scattering flux. In addition, the analysis above allows us to consider only the incompressible effects, by using the scattering wave field that excites the incompressible (dashpot) mode and by considering the incompressible radiation equation. These considerations are formulated below:

$$\begin{aligned} &\tfrac{\omega^2}{g}\phi^{SI} + \tfrac{\partial \phi^{SI}}{\partial y} = 0 \\ &\tfrac{\omega^2}{g}\phi^{RI} + \tfrac{\partial \phi^{RI}}{\partial y} = \begin{cases} 0 & \text{for} \quad x \geq b \qquad \text{(outside the OWC)} \\ \frac{\omega}{\rho_w g} p^I & \text{for} \quad 0 \leq x \leq b \quad \text{(inside the OWC)} \end{cases} \end{aligned} \tag{47}$$

where ϕ^{SI} is the scattering potential corresponding to the incident wave field that excites only the incompressible (dashpot) response. Equation (47) is in the form of the dynamic boundary condition considered in [5], and by further introducing a PTO resistance coefficient such as:

$$K' = \tfrac{K}{\sqrt{1+\Omega^2}}. \tag{48}$$

We can write a linear relation between p^I and the velocity at the resistance layer:

$$p^I = K' \tfrac{\partial \phi^I}{\partial y} = K' \left(\tfrac{\partial \phi^{SI}}{\partial y} - \tfrac{\partial \phi^{RI}}{\partial y} \right). \tag{49}$$

The fully coupled problem, presented in equations (28)- (36) can be solved by using techniques similar to those in [6] and [5] but we do not pursue that here. Equations (47)-(49) form the dynamic boundary condition for the incompressible mode. Treating the incompressible mode separately is advantageous for two reasons: i) we can assess the energy efficiency of the OWC using methodologies designed for incompressible flows (e.g. [5]), as energy production is related only to incompressible processes, and ii) we can facilitate the derivation of scaling recommendations, as will be shown in the next section.

3.2. ***Energy processes***

During wave interaction with OWC, the incident wave energy is transmitted inside the chamber, exciting the free-surface motion inside the OWC and subsequent pneumatic processes related to air compression and energy consumption at the PTO. In this section the effect of the air compressibility in limiting the available wave energy for conversion into power is demonstrated, as well as the infuence of compressibility effects to determining the optimal PTO resistance.

The available power that can be consumed at the PTO can be calculated throguh the incident wave field as follows:

$$\bar{E}_w = \frac{1}{16}\rho g H^2 c_g \tag{50}$$

where E_w is the total incident wave power and c_g the group velocity of the incident wave train. According to the analysis in the previous section, the incident wave field can be decomposed to two components, exciting the compressible and the incompressible mode, respectively. The scattering incompressible mode represented by $\Lambda^I q^S$ (see equation (40)) is the only one relevant to energy consumption at the PTO. For the purposes of this study, we will argue that for a given wave frequency and OWC shape, the interface amplitude is directly proportional to the incident wave amplitude, this is a reasonable assumption, especially for the linear analysis in the present work, as in this case, wave heights and amplitudes act as scaling parameters of the velocity potential. Therefore, the ratio of the incident wave height corresponfing to the scattering incompressible mode H^I is related to the total incident wave height H as follows:

$$H^I/H = \frac{|q^{SI}|}{|q^S|} = |\Lambda^I| \tag{51}$$

where $q^{SI} = \Lambda^I q^S$. Solving equation 51 for H^I gives

$$H^I = \frac{H}{\sqrt{1+\Omega^2}} \tag{52}$$

According to the analysis of [5] and [24] the efficiency n of the OWC can be expressed through the ratio of the energy captured at the PTO to the total

incident wave energy, therefore

$$n = \frac{\bar{E}_{OWC}}{\bar{E}_w} \tag{53}$$

where

$$\bar{E}_{OWC} = \frac{1}{T}\int_0^T p(t)q(t)\cdot dt = \frac{1}{T}\int_0^T K\bar{v}^2(t)b\cdot dt \tag{54}$$

is the power captured at the PTO.

Let n' be the efficiency of the OWC calculated assuming incompressible flow, then combining equations (52) and (53) it is derived:

$$n = \frac{n'}{1+\Omega^2} \tag{55}$$

Given that n' can be bounded by $[0, 1]$ then n is bounded by $[0, \frac{1}{1+\Omega^2}]$. This essentialy means that the effect of air compressibility limits the energy available to be captured at the OWC, as part of the incident wave energy is directed towards exciting compressible processes in OWC's, where no significant energy consumption takes place.

With respect to the influece of the compressibility to the optimal PTO configuration, the analysis of [5] calculates the optimal resistance coefficient K'_{opt} as a function of the width of the OWC and wave characteristics, through the quantities of radiation admittance and susceptance. This analysis is applied only for incompressible flow so we can calculate the resistance coefficient including the influence of the incompressible flow using equation (48). Remembering that Ω is linearly related to K and solving for the optimal PTO resistance, including compressible effects, gives:

$$K_{opt} = \frac{K'_{opt}}{\sqrt{1-(\Omega'_{opt})^2}} \tag{56}$$

where $\Omega'_{opt} = K'_{opt}\omega h/\gamma p_o$. It can be shown that $\Omega'_{opt} < 1$ from equation (48) by considering $K = K_{opt}$, $K' = K'_{opt}$ and multiplying both parts with $\omega h/\gamma p_o$. Equation (56) suggests that by taking into account the compressibility effects, the optimal PTO resistance coefficients is increased compared to the one calculated by [5], by assuming incompressible flow.

4. Scaling of air compression

4.1. Applying Froude Scaling

In this section, we investigate the influence on our mathematical model of applying Froude scaling to the description of the water flow. First we define the global Froude scale constant s_F

$$s_F = L_P/L_M \tag{57}$$

where L_M is the significant length in the model and L_P is the corresponding length in the prototype. Hereafter we use subscripts M and P to denote model and prototype scale, respectively. According to Froude scaling, the OWC properties K, ω, and h are scaled as follows: $K_M = K_P/\sqrt{s_F}$, $\omega_M = \omega_P\sqrt{s_F}$ and $h_M = h_P/s_F$, respectively. By applying these relations to definition (14), we find that the compression numbers for the prototype and model scale differ in the ratio:

$$\frac{\Omega_M}{\Omega_P} = 1/s_F. \tag{58}$$

Equation (58) makes clear that using a global Froude scale incorrectly scales compressibility, as Ω changes with scale. By leaving the height of the OWC unscaled ($h_M = h_P$), it is observed that $\Omega_P = \Omega_M$. This is consistent with the suggestions of [10], for including compression effects in an OWC physical model. This, however, is an impractical solution and in [10] alternatives are discussed about including compression effects by increasing the available air volume or implementing active control to the volume variations.

The potential flow equations can be used to inform us of the implications of using Froude scaling, as they are satisfied in all scales. Nearly all the equations for potential flow remain unchanged by interaction with the air phase, such as Laplace 's equation (28), the kinematic boundary condition (30) and the dynamic boundary condition outside the OWC (31); all these are automatically satisfied at all Froude scales. Therefore, scaling effects are introduced through the dynamic boundary condition in the OWC, which is further decomposed into

scattering and radiation components, according to equation (35). In the latter we observe that the scattering potential obeys Froude scaling laws, which is expected, as this component concerns the interaction with the OWC without air pressurisation. By contrast, pressure variables in the radiation components of equation (35) are influenced by the compression number, which, as we have demonstrated in (58) depends on the Froude scale. In order to further investigate the influence of scaling, from equations (40) and (41) we consider the pressure amplitude in the chamber:

$$p_c = K\bar{v} = K\frac{\partial \phi^I}{\partial y} = K\left(\Lambda^I \frac{\partial \phi^S}{\partial y} - \frac{\partial \phi^{RI}}{\partial y}\right) \tag{59}$$

which we can also write

$$p_c = K\frac{\partial \phi^I}{\partial y} = i\Omega K\frac{\partial \phi^C}{\partial y} = i\Omega K\left(\Lambda^C \frac{\partial \phi^S}{\partial y} - \frac{\partial \phi^{RC}}{\partial y}\right). \tag{60}$$

By combining equations (59), (60) and (35), new relations for the scattering, incompressible and compressible radiation are obtained:

$$\begin{aligned}
&\tfrac{\omega^2}{g}\phi^S + \tfrac{\partial \phi^S}{\partial y} = 0 \\
&\tfrac{\omega^2}{g}\phi^{RI} + \left(1 + S^\Omega\right)\tfrac{\partial \phi^{RI}}{\partial y} = S^\Omega \Lambda^I \tfrac{\partial \phi^S}{\partial y} \\
&\tfrac{\omega^2}{g}\phi^{RC} + \left(1 + i\Omega^2 S^\Omega\right)\tfrac{\partial \phi^{RC}}{\partial y} = S^\Omega \Lambda^C \tfrac{\partial \phi^S}{\partial y}
\end{aligned} \tag{61}$$

where

$$S^\Omega = \frac{K\omega}{\rho_w g\sqrt{1+\Omega^2}} \tag{62}$$

Equations (61) must be valid at prototype and model scale. The condition that satisfies this requirement for all radiation components is $\Omega_P = \Omega_M$, which is impossible to achieve with Froude scaling, as shown in equation (58). From the latter, we also deduce that by using Froude scaling (assuming $s_F > 1$), $\Omega^2 S^\Omega$ and Λ^C are larger at model scale than prototype, while S^Ω and Λ^I are larger at prototype scale than the model scale. Therefore, during the conversion

from prototype to model scale, the compressible radiation contribution will be underpredicted, and the incompressible radiation will be overpredicted.

Overpredicting the incompressible radiation component at model scale leads one to being over-optimistic about the energy output of an OWC. In addition, using Froude scaling for the resistance does not ensure that the optimal frequency regime will be correctly estimated using small scale models. These two remarks are further investigated in the following section, where recommendations for the correct scaling of the energy output of an OWC are given.

4.2. Scaling recommendations

As we have demonstrated in (48 and 49), it is possible to manipulate the scattering and incompressible radiation equations in order to obtain the same as those encountered in [5], by using the concept of the scattering potential that excites the incompressible mode and the equivalent resistance. Combining these with equations (61) and (62), we obtain:

$$\begin{aligned} &\tfrac{\omega^2}{g}\phi^{SI} + \tfrac{\partial \phi^{SI}}{\partial y} = 0 \\ &\tfrac{\omega^2}{g}\phi^{RI} + \left(1 + S^{\Omega}\right)\tfrac{\partial \phi^{RI}}{\partial y} = S^{\Omega}\tfrac{\partial \phi^{SI}}{\partial y} \end{aligned} \tag{63}$$

where

$$S^{\Omega} = \frac{K'\omega}{\rho_w g} \tag{64}$$

Equations (63) and (64) are not explicitly dependent on Ω, and we can therefore apply Froude scaling to all the variables involved, including K' and ϕ^{SI}. So, given a particular OWC design at prototype scale, the scaling of the energy output at Froude model scale will be consistent if the following conditions on K' and the incident wave amplitude are met:

$$K'_M = \tfrac{K'_P}{\sqrt{s_F}} \quad \text{and} \quad \phi^{SI}_M = (s_F)^{-3/2}\phi^{SI}_P \tag{65}$$

By combining the definition of the equivalent resistance (48) and the scaling relation in (65) we calculate the PTO resistance in model as:

$$K_M = \sqrt{\frac{\sqrt{1+4A_M C_M}-1}{2A_M}} \tag{66}$$

where

$$A_M = \frac{\omega_M^2 h_M^2}{\gamma p_o} = \frac{1}{s_F}\frac{\omega_P^2 h_P^2}{\gamma p_o} \qquad \text{and} \qquad C_M = \frac{1}{s_F} K_P^2 (1+\Omega_P^2) \tag{67}$$

Assuming that under typical operating conditions in small scale OWC models $\Omega_M << 1$, then $K'_M = K_M$. Thus, from equation (66) we derive:

$$K_M = \frac{K_P}{\sqrt{s_F(1+\Omega_P^2)}} \tag{68}$$

Evans and Porter [5] derive an expression for the optimum PTO resistance, which we can use to calculate a value of K' for optimal energy efficiency. This means that the energy efficiency of the OWC depends on the compression number Ω. Nevertheless, scaling for the equivalent resistance eliminates this dependency, and using this scaling in small scale models can improve the consistency of the results, when converting to prototype scale.

Once the resistance parameter is defined, Ω_M is calculated, either to be used for further scaling calculations or to verify the assumption for equation (66). The scaling of the scattering potential that excites the incompressible mode is not as straightforward. **According to the analysis presented in Section 3.2**, let the incident wave height at prototype scale that excites the incompressible mode be:

$$H_P^I = \frac{H_P}{\sqrt{1+\Omega_P^2}} \tag{69}$$

where H_P is the total incident wave height. As argued before, we use Froude scaling of the incident wave height H_P^I rather than H_P, as this will ensure a consistent scaling of ϕ_{SI} both inside and outside of the OWC, thus ensuring the correct scaling of the energy output. This results in the model scale incident wave height H_M being scaled by the following equation

$$H_M = H_P \frac{\sqrt{1+\Omega_M^2}}{s_F\sqrt{1+\Omega_P^2}} \tag{70}$$

or, if Ω_M is much less than one, then approximately

$$H_M = H_P \frac{1}{s_F \sqrt{1+\Omega_P^2}}. \tag{71}$$

It is thus demonstrated that in order to ensure a consistent scaling for the energy output production, a different scaling procedure has to be applied for the PTO resistance and the incident wave height in the physical model, otherwise scaled by Froude laws. While the resistance scaling is straightforward for physical modellers, scaling the incident wave height with a law different that Froude scaling may prove inconvenient as emerging nonlinearities in shallow water (close to the OWC) may cause substantially different evolution of nonlinear wave shoaling and breaking that may invalidate the prediction of wave loads, especially for extreme wave conditions. Alternatively, we can leave the Froude scale for ϕ^S and adjust for the contribution of the incompressible mode. So, considering the validity of equation (63) across scales, we can calculate a modified scaling factor for the incompressible radiation effects

$$s'_F = s_F s_\Omega \tag{72}$$

where we define

$$s_\Omega = \frac{1+\Omega_M^2}{1+\Omega_P^2} \tag{73}$$

The scaling factor s'_F can replace Froude scaling factor s_F for all variables directly related to the incompressible radiation problem, such as the interface elevation of the incompressible mode ($\eta_P^I = s'_F \eta_M^I$) or any potential related to the incompressible mode ($\phi_P^{I,SI,RI} = (s'_F)^{\frac{3}{2}} \phi_P^{I,SI,RI}$).

It can be shown from (49) that scaling for the equivalent resistance and the total incident wave field, ϕ^s, ensures Froude scaling for the pressure

$$p_P = s_F p_M. \tag{74}$$

Scaling for the compressible radiation properties can be indirectly achieved by using the relations between incompressible and compressible properties that

were developed in sections 2 and 3. For example, the total elevation amplitude of the interface inside the OWC can be derived as a function of the amplitude corresponding to the incompressible mode as follows:

$$\eta_P = \frac{s'_F}{\sqrt{s_\Omega}}\eta_M. \tag{75}$$

Finally, the power output is proportional to $\bar{E} \sim p\frac{\partial \eta^I}{\partial t}$, therefore

$$\bar{E}_{OWC} = s_F\sqrt{s'_F}\bar{E}_P. \tag{76}$$

In terms of scaling extreme wave loads, this proves to be more complicated, as the following properties must be correctly scaled:

- Air pressure
- Hydrodynamic pressures inside the OWC
- Hydrodynamic pressures outside the OWC
- Phase differences between all the items above

We can use equations (74)-(75) to scale the air pressure and hydrodynamic pressures inside the OWC, assuming that they are proportional to the amplitude. In addition equation (16) is used to calculate the phase difference between the air pressure and the free-surface oscillation. For the hydrodynamic pressures outside the OWC, we need first to calculate the total (incident and reflected) amplitude of the OWC. The reflection coefficient can be defined as the square-root of the ratio of the wave energy that is reflected offshore.

$$R = \sqrt{1 - \frac{\bar{E}_{OWC}}{\bar{E}_I}} \tag{77}$$

and the reflection coefficient for the prototype scale is calculated from model scale properties as follows:

$$R_P = \sqrt{1 - \frac{\bar{E}_{OWC(M)}}{\sqrt{s'_F}\bar{E}_{I(M)}}}. \tag{78}$$

The reflection coefficient in equation (78) provides information about the average reflected wave height, nevertheless a complete solution of the system of equation (35) is required to define the evanescent modes of the incident and reflected wave field that define the total wave height outside the OWC and the phase difference between the wave field and the OWC oscillation. Since a complete solution is not attempted in this paper, accounting for the effects of scaling on the extreme loads is not presented in this work.

In this section, accounting for the effects of scaling in OWC due to air compression is attempted using an analytical approach. It is therefore important to point out the limitations of this method, which are caused by nonlinearities in the air compression response (see [14]), nonlinearities in the incident wave field, as well as disregarding intense free-surface dynamics that lead to impulsive loading inside and outside the OWC. In addition, the use of the compression number is developed by considering a regular wave field, with one value for frequency ω, whereas random waves nedd to be considered for designing an OWC. If the waves have a relatively narrow band of frequencies, then we may choose a value of ω in the centre of the band. If the wave spectrum range is broad, it would pay to treat several values of ω corresponding to the load peaks or spread of frequencies.

The analysis above did not take into account active PTO control for optimising energy capture during interaction with random waves [27]. This could be included using an methodology for incompressible air flow e.g. [28], but considering only the incident wave height related to the incompressible mode and K' as the resistance coefficient as starting points. Note that for relatively broad-band spectra, K' will be relatively dependent on Ω for each individual wave or wave groups, so further investigation should be performed to define the variation of Ω with respect to each wave group. This, nevertheless should not introduce more control parameters to the optimisation algorithm, apart from constants h and γp_o.

4.3. Effects of sea water scaling

Fresh water rather than sea water is typically used in physical modelling of coastal structures, causing an additional scaling effect, due to density differences between sea and fresh water. In most coastal structures, these scaling effects can be included a posteriori, for example by multiplying wave loads with a correction ratio accounting for the effect of sea water. In our study, differences in water density introduce scaling effects in the interaction between air and water phase as for example the radiation component in equation (29) includes the water density. These effects can be resolved in a relatively simple manner if we introduce the following variable:

$$I' = \frac{K'}{\rho_w g} \tag{79}$$

where I' is a resistance coefficient normalised to the specific weight of the water. Equation (64) then becomes:

$$S_\Omega = I'\omega \tag{80}$$

Froude scaling can be now applied with respect to I' according to (82)

$$I'_M = \frac{I'_P}{\sqrt{s_F}} \tag{81}$$

Assuming sea water density applies always in prototype scale and fresh water always in model scale, the scaling relation for K' becomes:

$$K'_M = s_\rho \frac{K'_P}{\sqrt{s_F}} \tag{82}$$

where s_ρ is ratio of sea water to fresh water. The PTO resistance is then defined by scaling relation (66), assuming

$$A_M = \frac{(s_\rho)^2}{s_F}\frac{\omega_P^2 h_P^2}{\gamma p_o} \qquad \text{and} \qquad C_M = \frac{(s_\rho)^2}{s_F} K_P^2(1+\Omega_P^2) \tag{83}$$

For $\Omega_M << 1$, the scaling relation can be calculated according to Equation (84)

$$K_M = \frac{s_\rho K_P}{\sqrt{s_F(1+\Omega_P^2)}} \tag{84}$$

Density scaling effects can be further included in the analysis of Section 4.2, by replacing Equation (67) with (83) and (68) with (84). Since scaling of K_M

already includes the effect of sea water scaling, this is also included in any relation containing Ω_M, as the latter is derived by the former for the model scale.

5. Validation and example applications

In this section, the method is validated using numerical and experimental data originally presented in [26, 29, 23] and subsequently, example applications are presented from other physical model tests e.g. [24] and prototype OWC structures, such as the Pico Power Plant [30, 31]. For the purposes of all calculations, it is assumed that γp_o=140kPa.

5.1. Validation

The experimental configuration of the physical model tests in the Grosse Welle Kanal (GWK) is presented in [26, 29, 23] in detail. The OWC structure comprises three rectangular chambers 1.44 m x 2.45 m each, with the longer dimension being aligned with the longitudinal axis of the flume. The PTO casing was represented by using a 0.5 m diameter pipe attached to the roof of the OWC and the PTO resistance with an orifice plate inserted in the middle of the pipe. A set regular and random wave conditions were tested combined with different orifice diameters varying from 0.05 m to 0.3 m, to investigate the effect of different PTO configurations. Herein, we use an example of a regular wave condition with $T = 4$ s, H=0.4 m and still water depth at the generation d_G=3.5 m, which corresponds to d =1.58 m at the toe of the structure. Since the total height of the OWC chamber is 2.4 m, the height of the air column is calculated to be h=0.82 m. Two orifice plate diameters are considered, 0.05 m (Case 1) and 0.3 m (Case 2), and significant compressibility effects are anticipated to occur for the former one (0.05 m), due to the high flow resistance at the orifice.

Both the free-surface elevation inside the OWC chamber and the pressure drop at the orifice were recorded and shown in Figure 5.1. Data were processed using a 60 s window (15 waves), where the regular waves were fully developped.

To clean up the noise from the measurements, a low-pass filter at $T/10$ was applied. The compression number, Ω was calculated experimentally using two methods:

- By manipulating equation (13) to calculate Ω as follows:

$$\Omega = \frac{1}{\sqrt{\left(\frac{\bar{\eta}_c \gamma p_o}{p_c h}\right)^2 - 1}} \tag{85}$$

- By considering the phase difference α_η and equations (15) and (16) to calculate Ω as follows:

$$\Omega = \arctan(\frac{\pi}{2} - \alpha_\eta) \tag{86}$$

Note that α_η is calculated as the phase difference between the signal of the pressure and the free surface elevation, considering the primary harmonic of the wave motion, herein at T =4 s. The calculation of Ω using equation (85) is performed using both using the data presentend at Figure 5.1 as well as by considering only the primary harmonic of both the free surface and the pressure drop.

The compression number Ω was also calculated theoretically using equation 14. Since the pressure drop is quadratic to the velocity, the K was calculated using the linearisation method proposed in Section 2.4. The amplitude of the velocity $\bar{u}_m$, was therefore computed using the following relation

$$\bar{u}_c = S_b \sqrt{\frac{p_c}{K_o}} \tag{87}$$

where S_b is the ratio of the OWC chamber area to the pipe area and K_o is calculated according to equation (90) [32]:

$$K_o = [1 - (S_o)^2 C_c]^2 \frac{1}{(S_o)^4 (C_c)^2} \tag{88}$$

where S_o is the ratio of the orifice diameter to the pipe diameter (0.1 and 0.3 for Case 1 and Case 2, respectively) and C_c is an empirical coefficient calculated according to [32] (0.62 and 0.66 for Case 1 and Case 2, respectively).

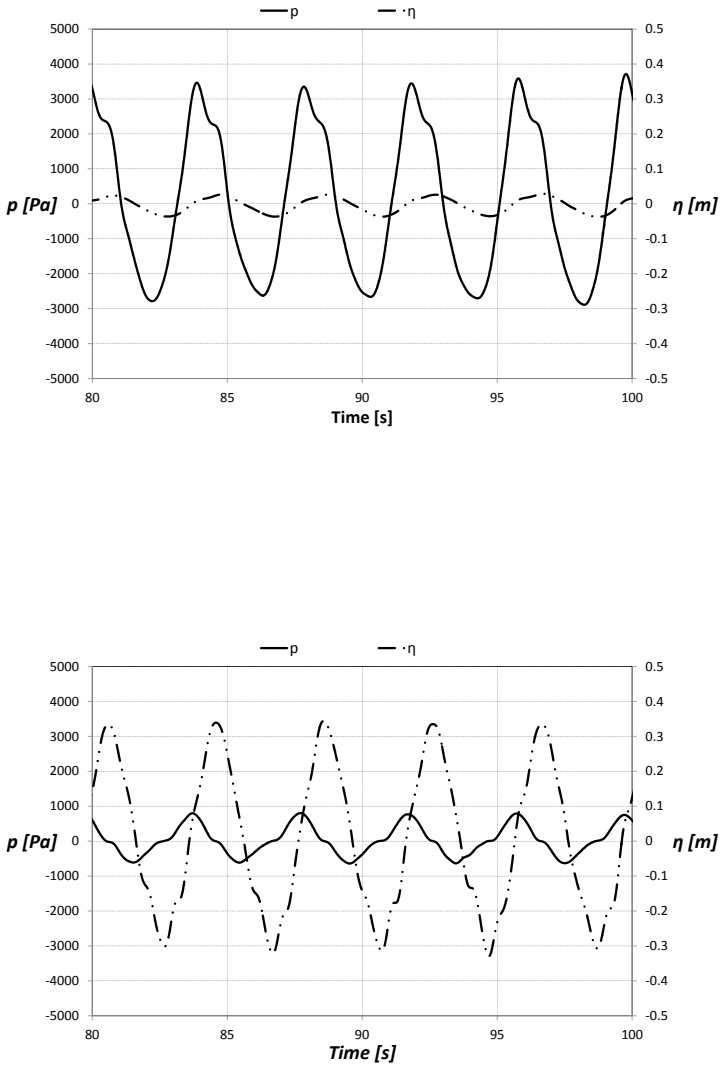

Figure 6: Time series of free-surface elevation (dashed lines) and pressure (solid lines) for Case 1 (top) and Case 2 (bottom). Pressure values are shown at the left axis, whilst free-surface elevation values are shown at the right axis

The pressure drop amplitude p_c in equation 87 is calculated from the experimental data, by considering only the amplitude of the primary harmonic and $\bar{v}_m$ is calculated using equation (26). Results are presented in Table 5.1. Based on these results, the following comments are made:

- The theoretical analysis is in accordance with the findings from the experimental analysis.
- The compression number Ω is accurately calculated for Case 1
- Results from experimental analysis using the primary harmonics are very similar to the ones derived by including higher-order terms, hence demonstrating that applying linearisatin is a reasonable assumption.
- The calculation of Ω is less accurate for Case 2. This is probably because uncertainties such as the empirical calculation of resistance or emergence of nonlinearities are probably magnified due to the fact that $\Omega \simeq 0$. In practice though, both the experimental and the theoretical calculation of Ω demonstrate that the air flow in Case 2 is characterised as incompressible.
- When the pressure drop is related to the velocity quadratically, a calculation of the vertical velocities in the OWC chamber is necessary to obtain a value for K. In this case, we were able to calculate it directly from the experimental data. In the absence of pressure and velocity data, the calculation can be achieved by guessing the efficiency related to incompressible processes $0 \leq n' \leq 1$ and calculating $\bar{v}_c$ using equations (50)-(56). As Ω is part of the calculation procedure.

5.2. Example applications

5.2.1. OWC experiments in UWA [24]

The experimental tests were performed in a 50m long and 1.5m wide wave flume at the University of Western Australia (UWA). The structure comprises a caisson-shaped OWC with a rectangular opening at the offshore face and a

Variable	**Case 1**	**Case 2**
$\bar{u}_m$ (m/s)	0.015	0.34
K (theoretical, Pa·s/m)	77200	675
Ω (theoretical)	0.71	0.006
Ω (unfiltered, using $p_c/\bar{\eta}_c$)	0.71	0.012
Ω (filtered, using $p_c/\bar{\eta}_c$)	0.70	0.013
Ω (using a_Ω from peak frequency)	0.72	0.05
K calculated from Ω (unflitered, Pa·s/m)	77200	1255

5 mm wide rectangular opening located at the top face, 5 cm away from the back wall. Both openings practically extend at the full width of the flume, thus making the configuration two-dimensional. The width of the chamber is b =0.64 m. Whilst the height of the air column is not explicitily mentioned in [24], based on evidence from drawings and photographs, this is assumed to be 0.7 m.

The authors in [24] present results for the energy efficiency n and we can therefore use equations (50), (53) and (54) to calculate $\bar{v}_c$ and subsequently $\bar{v}_m$. Combining the aforementioned equations and calculating the integral in (54) gives:

$$\bar{u}_c = 0.5\pi\bar{u}_m = \sqrt[3]{\frac{3\pi E_{OWC}}{4K_2 b}} \tag{89}$$

where K_2 is calculated from the [32] as

$$K_2 = [1-(S_b)C_c]^2\frac{1}{(S_b)^2(C_c)^2} \tag{90}$$

where S_b is the ratio of the width of the PTO opening to the OWC width and C_c is 0.61. The wave energy captured at the PTO is calculated as $E_{OWC} = nE_w$, where n is taken from the derived efficiency curve in [24] and E_w is calculated from the incident wave field using equation 50. The compression number was calculated for H =0.1m and T =1, 1.5 and 4 s, and was found to be Ω =0.013, 0.019 and 0.008 respectively, using $n \simeq$ 0.1, 0.7 and 0.5, respectively (results summarised in Table 1). This means that in the experiment of [24], the

Table 1: Wave characteristics, K, $\bar{v}_m$ and Ω for the OWC experiments in [24].

ω (s$^-$1)	h (m)	K_2 (kg$\cdot$ m $^{-3}$)	$\bar{v}_m$ (m/s)	K (Pa $\cdot$ s/m)	Ω
6.28	0.7	26167	0.015	400	0.013
4.19	0.7	26167	0.035	913	0.019
1.57	0.7	26167	0.039	1029	0.008

compressibility effects were not significant. It is nevertheless stated that the prototype structure is expected to be at 12.5 scale and in this case, we would anticipate that $\Omega_P \simeq 0.1 - 0.25$, which suggests that the air compressibility effects will be marginally significant at prototype scale, assuming that the PTO orifice used in the laboratory is sufficiently representative of the prototype one.

5.2.2. Pico power plant [30, 31, 33]

The OWC structure from the Pico power plant in Azores, Portugal is used as an example [30]. In this case, Wells turbine is used as PTO, therefore $K = K_1$. The linear damping coefficient with respect to the air flow discharge was set to 120 Pa $\cdot$ s/m^3. The PTO resistance has to be therefore converted to match the resistance layer assumption, as introduced in the current paper using the following relation:

$$K = bK_q \tag{91}$$

where K_q=120 Pa $\cdot$ s/m^3 is the of proportionality between the volume flux and the pressure drop at the resistance layer and b is the horizontal cross-sectional area of the OWC. According to equation (91), K = 17280 Pa$\cdot$s/m. The cross-sectional area of the chamber at mean sea level (MSL) is square with size 12 m $\times$ 12 m. Since the cross-sectional area varies along the OWC height, the effective height of the air column is calculated by dividing the total volume of the air above MSL V_o to the width of the OWC b. It is estimated from [30] that $V_o \simeq$1200 m^3, therefore the effective height is $h = V_o/b \simeq 8$ m. The design period is set to 12 s [33]. It is calculated that Ω=0.5, therefore in Pico powerplant,

Table 2: Wave characteristics, K and Ω for the OWC-WEC at Pico, Azores

ω (s$^-$1)	h (m)	K (s^{-1})	Ω
0.52	8	17280	0.5

compressible effects are clearly of significance. Results are summarised in Table 2.

According to these results and in combinations with the analysis in Section 3.2, the compressibility effects will limit the of the available wave energy to about 80% of the maximum theoretical, as part of the incident wave energy will be associated with the cycle of the net air compression and expansion, thus becoming unavailable for exploitation. Note that this percentage corresponds to wave energy concentrated aroung a period of 12 s, and the percentage will change for different periods, i.e. for wave period of 6 s, this would reduce the available wave energy for conversion to about 50% of the incident wave energy.

6. Discussion and recommendations for use

In this work, we propose the use of a (nondimensional) compression number Ω, for the air flow characterisation inside the OWC. The compression number defined by equation (14), represents the relative importance of air compression effects and thus can be used to characterise the flow inside an OWC. This number is derived, through linear analysis, from the thermodynamic equations of the air phase. We have shown that when the compression number is sufficiently small (e.g. $\Omega \leq 0.1$) then the air flow can be considered as incompressible, whereas when $\Omega >> 10^{-1}$, air compressibility is significant. These effects are manifested as changes between the magnitude and the phase difference between the volume fluxes at the air-water interface and the resistance layer.

These effects can only be investigated by considering the coupled problem of wave interaction with the OWC structure and response of the PTO. Therefore, the air compressibility is introduced to the potential flow equations for the water phase through the air-water dynamic boundary condition inside the OWC. The

latter is decomposed into scattering and radiation problems, following [5]. It is shown that changing the scale affects both the performance of the OWC (through the development of differences between the fluxes in the resistance layer and the free-surface elevation), and alters the OWC resonance characteristics. Scaling effects are further investigated by manipulating the equations to match the incompressible form proposed in [5] and then applying Froude scaling to the modified equations. This yields some scaling relations that, when applied to a small scale model, would ensure a consistent and predictable scaling of the energy performance. Scaling effects in relation to maximum wave loading have yet to be resolved, as a full solution of the potential problem should be pursued.

The methodology for characterisation was applied to practical applications. First, the analysis is validated using experimental data from [26, 29, 23]. Key processes predicted by the analysis, such as the free-surface motion compressing the air, and the development of phase differences, were also proved by analysing the experimental data. Despite the linear nature of the methodology proposed, quantitative comparisons also yielded very good results. Consequently it was used to assess compressibility effects in model scale [24] and in prototype scale. It is confirmed that in experiments compressibility effects are generally negligible, except when the flow at the PTO is highly restricted. By contrast, compressibility effects are relatively important in operational OWC configurations in prototype scale, and can lead to a reduction in efficiency, especially in the conversion of wave energy to pneumatic energy.

The importance of introducing these new concepts (and especially the compression number) lies in the chance to assess the importance of the compression effects by performing a simple calculation, as shown in equation (14). The compression number is also useful to assess the quality of numerical and physical modelling, and in particular:

- In physical modelling, the procedure developed in Section 4.2 can be used

to estimate the influence of power take off on the compressibility of air and its scaling from model to prototype;

- In computations, the simple 2D OWC geometry can be reproduced with a numerical model that accounts for air compression, and the model can be validated against the predictions developed in Section 2.

The methodology that we propose is subject to some limitations due to the nature of the linear equations and the consideration of regular waves or narrow-band. Whilst initital comparison showed that the theoretical analysis is in accordance with large scale physical modelling data, it will be useful if the predictions arising from this methodology are further compared with large scale physical modelling data that include random wave tests, such as the ones presented in [23], to quantify the extent that such a simple characterisation is representative of a random wave field. In addition, a more extensive investigation is required, using numerical modelling and small and large scale experimental data as well as field measurements to attain the range of validity of the theoretical considerations developed within this work.

Acknowledgements

Aggelos Dimakopoulos would like to acknowledge the financial support from HR Wallingford's internal research project CAY0490. He thanks Prof. William Allsop for his continuous encouragement and support and Gillaume Maret, visiting researcher in HR Wallingford, for commenting on an earlier version of the text and the equations. Mark Cooker thanks UEA for leave to pursue this research. Tom Bruce acknowledges the support of University of Edinburgh during this work. In the course of writing this paper, part of the analysis was presented at the European Wave and Tidal Energy Conference 2015 in Nantes, France. The authors gratefully acknowledge the constructive feedback and comments received from Prof. Antonio Falcao.

References

[1] T.V. Heath, A review of oscillating water columns, Philosophical Transactions of the Royal Society of London 370 (2012) 235–245.

[2] D.V. Evans, The oscillating water column wave-energy device, Journal of the Institute of Mathematics and its Applications 22 (1978) 423–433.

[3] J. N. Newman, Interaction of water waves with two closely-spaced vertical obstacles, Journal of Fluid Mechanics 66 (1974) 96 – 106.

[4] A. J. N. A. Sarmento, A. F. d. O. Falcao, Wave generation by an oscillating surface-pressure and its application in wave-energy extraction, Journal of Fluid Mechanics 150 (1985) 467–485.

[5] D.V. Evans, R. Porter, Hydrodynamic characteristics of an oscillating water column device, Applied Ocean Research 17 (1995) 155–164.

[6] D.V. Evans, Wave-power absorption by systems of oscillating surface pressure distributions, Journal of Fluid Mechanics 114 (1982) 481–499.

[7] R. Porter, D.V. Evans, Complementary approximations to wave scattering by vertical barriers, Journal of Fluid Mechanics 294 (1995) 155–180.

[8] C. M. Smith, Some problems in linear water waves, Ph.D. thesis (1995).

[9] A. Mora, F. Bautista, F. Mendez, Influence of a tapered and slender wave collector on the increment of the efficiency of an oscillating water column wave-energy converter., Ocean Engineering 129 (2017) 20 – 37.

[10] J. Weber, Representation of non-linear aero-thermodynamic effects during small scale physical modelling of owc wecs, in: Proceedings of the 7th European Wave and Tidal Energy Conference, 2007.

[11] J. Weber, Optimisation of the hydrodynamic-aerodynamic coupling of an oscillating water column wave energy device, Ph.D. thesis (2006).

[12] W. Sheng, R. Alcorn, T. Lewis, Physical modelling of wave energy converters, Ocean Engineering 84 (2014) 29 – 36.

[13] A. F. Falcao, J. C. Henriques, Model-prototype similarity of oscillating-water-column wave energy converters, International Journal of Marine Energy 6 (2014) 18 – 34.

[14] W. Sheng, F. Thiebaut, M. Brooks, A. Lewis, R. Alcorn, Investigation of air compressibility of oscillating water column wave energy converters, in: Proceedings of 32nd International Conference on Ocean, Offshore and Arctic Engineering, 2013.

[15] E. Medina-Lopez, A. Monino Ferrando, M. Clavero Gilabert, C. del Pino, M. Losada Rodriguez, Note on a real gas model for owc performance., Renewable Energy 85 (2017) 588 – 597.

[16] H. Martin-Rivas, C. Mei, Wave power extraction from an oscillating water column at the tip of a breakwater, Journal of Fluid Mechanics 626 (2008) 395 – 414.

[17] Jean-Roch Pierre Nader, Interaction of ocean waves with oscillating water column wave energy convertors, Ph.D. thesis (2013).

[18] G. Cuomo, W. Allsop, S. Takahashi, Scaling wave impact pressures on vertical walls, Coastal Engineering 57 (6) (2010) 604 – 609.

[19] J. Falnes, Ocean Waves and Oscillating Systems, Cambridge University Press, 2002.

[20] A. F. Falcao, P. Justino, Owc wave energy devices with air flow control, Ocean Engineering 26 (1999) 1275 – 1295.

[21] J. Kestin, A course in thermodynamics, 3rd Edition, Vol. 1, Hemisphere Publishing, 1966.

[22] R. Raghunathan, The wells air turbine for wave energy conversion, Progress in Aerospace Science 31 (1995) 355–386.

[23] A. Viviano, S. Naty, E. Foti, T. Bruce, W. Allsop, D. Vicinanza, Large-scale experiments on the behaviour of a generalised oscillating water column under random waves, Renewable Energy 99 (2016) 875 – 887.

[24] M. T. Morris-Thomas, R. J. Irvin, K. P. Thiagarajan, An investigation into the hydrodynamic efficiency of an oscillating water column, Journal of Offshore Mechanics and Arctic Engineering 129 (2007) 273 – 278.

[25] A. F. O. Falcão, J. C. C. Henriques, L. M. C. Gato, Air turbine optimization for a bottom-standing oscillating-water-column wave energy converter, Journal of Ocean Engineering and Marine Energy (2016) 1–14doi:10.1007/s40722-016-0045-7.

[26] N.W.H. Allsop, T. Bruce, V. Ferrante, V. Russo, D. Vicinanza, M. Kudella, Large scale tests on a generalised oscillating water column wave energy converter, in: Proceedings of the HYDRALAB IV Joint User Meeting, 2014.

[27] A. F. Falcao, J. Henriques, Oscillating-water-column wave energy converters and air turbines: A review, Renewable energy 85 (2016) 1391 – 1424.

[28] R. E. Hoskin, B. M. Count, N. K. Nichols, D. A. C. Nicol, Phase Control for the Oscillating Water Column, Springer Berlin Heidelberg, Berlin, Heidelberg, 1986, pp. 257–268.

[29] A.S Dimakopoulos, M.J. Cooker, E. Medina-Lopez, D. Longo, R. Pinguet, Flow characterisation and numerical modelling of owc wave energy converters, in: Proceedings of 15th European Wave and Tidal Energy Conference, 2015.

[30] EUROPEAN WAVE ENERGY PILOT PLANT ON THE ISLAND OF PICO, AZORES, PORTUGAL. PHASE TWO: EQUIPMENT, Tech. Rep. 873192, Community Research and Development Information Service (2000).

URL http://cordis.europa.eu/docs/publications/4769/47698021-6_en.pdf

[31] A.F. Falcao, The shoreline owc wave power plant at the azores, in: Wave Energy 2000, 2000.

[32] D. Miller, Internal Flow Systems, 2nd Edition, BHRA, 1990.

[33] Arup Energy, Oscillating water column wave energy converter evaluation report, Tech. rep., The Carbon Trust, Marine Energy Challenge (2005).